Structures of Zika virus NS2B-NS3 protease in complex with peptidomimetic inhibitors

Phoo, Wint Wint; Zhang, Zhenzhen; Wirawan, Melissa; Chew, Edwin Jun Chen; Chew, Alvin Bing Liang; Kouretova, Jenny; Steinmetzer, Torsten; Luo, Dahai

2018

Phoo, W. W., Zhang, Z., Wirawan, M., Chew, E. J. C., Chew, A. B. L., Kouretova, J., . . . Luo, D. (2018). Structures of Zika virus NS2B-NS3 protease in complex with peptidomimetic inhibitors. Antiviral Research, 160, 17-24. doi:10.1016/j.antiviral.2018.10.006

https://hdl.handle.net/10356/80153

https://doi.org/10.1016/j.antiviral.2018.10.006

Structures of Zika virus NS2B-NS3 protease in complex with peptidomimetic inhibitors

Wint Wint Phoo[1,2,3,#], Zhenzhen Zhang [1,2,#], Melissa Wirawan [1,2,#], Edwin Chew Jun Chen[1], Chew Bing Liang Alvin[1,2,4], Jenny Kouretova[5], Torsten Steinmetzer [5*], Dahai Luo[1,2,3*]

Affiliations

[1]Lee Kong Chian School of Medicine, Nanyang Technological University, EMB 03-07, 59 Nanyang Drive, Singapore 636921

[2]NTU Institute of Structural Biology, Nanyang Technological University, EMB 06-01, 59 Nanyang Drive, Singapore 636921.[3]School of Biological Sciences, Nanyang Technological University, 60 Nanyang Drive, Singapore 636921.

[3]School of Biological Sciences, Nanyang Technological University, 60 Nanyang Drive, Singapore, 637551

[4]NTU Institute of Health Technologies, Interdisciplinary Graduate School, Nanyang Technological University, RTP 02-07, 50 Nanyang Drive, Singapore 637553.

[5]Institute of Pharmaceutical Chemistry, Philipps University, Marbacher Weg 6, 35032 Marburg, Germany.

[#] These authors contributed equally to the study.

*Correspondence to: steinmetzer@uni-marburg.de ; luodahai@ntu.edu.sg ;

Keywords: Zika virus; NS3 protease; flaviviral protease; drug discovery; protease inhibitor; X-ray crystallography; peptide inhibitors;

Abstract

Zika virus NS2B-NS3 protease plays an essential role in viral replication by processing the viral polyprotein into individual proteins. The viral protease is therefore considered as an ideal antiviral drug target. To facilitate the development of protease inhibitors, we report three high-resolution co-crystal structures of bZiPro with peptidomimetic inhibitors composed of a P1-P4 segment and different P1′ residues. Compounds 1 and 2 possess small P1′ groups that are cleaved by bZiPro, which could be detected by mass spectrometry. On the other hand, the more potent compound 3 contains a bulky P1′ benzylamide structure that is resistant to cleavage by bZiPro, demonstrating that presence of an uncleavable C-terminal cap contributes to a slightly improved inhibitory potency. The N-terminal phenylacetyl residue occupies a position above the P1 side chain and therefore stabilizes a horseshoe-like backbone conformation of the bound inhibitors. The P4 moieties show unique intra- and intermolecular interactions. Our work reports the detailed binding mode interactions of substrate-analogue inhibitors within the S4-S1′ pockets and explains the preference of bZiPro for basic P1-P3 residues. These new structures of protease-inhibitor complexes will guide the design of more effective NS2B-NS3 protease inhibitors with improved potency and bioavailability.

1. Introduction

Zika virus (ZIKV) belongs to the flavivirus genus, which also includes other important human pathogens such as Dengue virus (DENV) and West Nile virus (WNV). Although most ZIKV infections cause no or very mild symptoms, in the long term, ZIKV infections pose a public health threat because of its association with neurological complications amongst infants and adults (Baronti et al., 2014; Bell, Boyle, & Petersen, 2016). Due to the recent outbreak, the World Health Organization declared ZIKV a world public health emergency in 2015. Hence, there is still a pressing need for antiviral treatments and vaccine development against ZIKV.

The 11 kb (+)ssRNA genome of ZIKV is first translated into a polyprotein which requires both host proteases and viral NS2B-NS3 protease, for cleavage into individual proteins. The non-structural protein NS3 together with NS2B co-factor is a serine protease (Chambers, Grakoui, & Rice, 1991; Chambers et al., 1990). The hydrophilic central region of NS2B cofactor is essential for the proper folding and enzymatic activity of NS3 and is flanked by *N*- and *C*-terminal transmembrane regions (Chambers, Nestorowicz, Amberg, & Rice, 1993; Clum, Ebner, & Padmanabhan, 1997; Li, Li, Wong, Liew, & Kang, 2015). The NS2B-NS3 protease cleaves the viral polyprotein at NS2A/NS2B, NS2B/NS3, NS3/NS4A, and NS4B/NS5 (Cahour, Falgout, & Lai, 1992). As the NS3 plays an indispensable role in viral replication, it is an attractive antiviral target (Kang, Keller, & Luo, 2017).

The active site of NS2B-NS3 is shallow and solvent-exposed, making it challenging for development of inhibitors (Erbel et al., 2006; Hammamy, Haase, Hammami, Hilgenfeld, & Steinmetzer, 2013; Noble, Seh, Chao, & Shi, 2012). Although peptidomimetic inhibitors with nanomolar potency against DENV and WNV were reported, limited availability of protein-inhibitor co-crystal structures has hindered the structure-based optimization of these inhibitors (Mueller, Yon, Ganesh, & Padmanabhan, 2007; Schuller et al., 2011; Yin, Patel, Wang, Chan, et al., 2006; Yin, Patel, Wang, Wang, et al., 2006). Structural studies to complement compound identification by HTS are pivotal for the rational development of more effective antivirals using various *in silico* techniques. Due to comparable substrate preferences for multi-basic sequences and structural similarity of ZIKV

NS2B-NS3 protease to the DENV and WNV NS2B-NS3, previously reported inhibitors for DENV and WNV proteases could potentially be effective against the ZIKV. Previous crystal structures of the flavivirus NS2B-NS3 protease have been obtained with constructs containing a glycine-rich artificial linker between NS2B and NS3 (Aleshin, Shiryaev, Strongin, & Liddington, 2007; Chandramouli et al., 2010; Erbel et al., 2006; Hammamy et al., 2013; Lei et al., 2016; Noble et al., 2012; Noble & Shi, 2012; Robin et al., 2009). Structures of the inhibitor-free enzymes revealed an open conformation where the *C*-terminal segment of the NS2B cofactor is flexible and disordered. The linked NS2B-NS3 constructs adopt the closed conformation only when bound with an inhibitor (Aleshin et al., 2007; Hammamy et al., 2013; Noble et al., 2012; Robin et al., 2009). Recently, our studies have shown that the glycine-rich artificial linker introduces steric hindrance and changes the inhibitor-binding mechanism (Phoo et al., 2016). This conclusion has been supported by additional biochemical and NMR studies, which also showed that the unlinked construct bZiPro is closer to the native state, has higher activity, and is more suitable for the identification of effective inhibitors (de la Cruz et al., 2011; Kim et al., 2013; Shannon et al., 2016).

The co-crystal structures of bZiPro with small molecule inhibitors and with di-peptide derivatives have been reported (Lei et al., 2016; Li et al., 2018; Li et al., 2017). These inhibitors are also effective against other flaviviruses such as WNV and DENV (Koh-Stenta et al., 2015; Lei et al., 2016; Nitsche et al., 2017; Weigel, Nitsche, Graf, Bartenschlager, & Klein, 2015). Therefore, structural characterization of ZIKV NS3 protease with different inhibitors could also be beneficial towards the design of pan-flaviviral NS3 protease inhibitor development. Currently, the structural characterization of the ZIKV protease with longer peptide inhibitors is not available. In this study we report three co-crystal structures of unlinked NS2B-NS3 protease from ZIKV (bZiPro) with different peptidomimetic inhibitors occupying S4 – S1′ pockets. These structures shed light on how the longer peptidomimetic inhibitors interact with bZiPro and would be helpful towards the structure based design of peptide inhibitors.

2. Materials and Methods

2.1 Protein purification

The bZiPro was purified as previously reported (Zhang et al., 2016). In short, the protein was purified in following steps, 1) immobilized metal affinity chromatography (IMAC) using Ni2+-NTA beads (Qiagen, USA), 2) His-tag removal by addition of thrombin to the eluted proteins and dialysis against gel-filtration buffer containing 20 mM HEPES pH 7.5, 150 mM NaCl, 5% glycerol, 2 mM DTT overnight, 3) size exclusion chromatography using HiLoad 16/600 Superdex 75 pg column (GE Healthcare, USA). Fractions were collected and concentrated in the gel filtration buffer.

2.2 Crystallization and structure determination

The bZiPro:compound complex (molar ratio 1:3) was incubated for 1 hour on ice at the protein concentration of 40 mg/ml. 1 µL of the mixture was mixed with 1 µL of reservoir solution (2 M ammonium sulfate, 0.1 M sodium acetate trihydrate pH 4.6) and incubated at 18 °C in a hanging-drop vapor diffusion experiment. Crystals appeared after two days and were cryoprotected using reservoir solution with 20% glycerol before being flash-cooled in liquid nitrogen.

Diffraction intensities were collected at Australian Synchrotron (Clayton, Victoria) with the MX2 beamline and Swiss Light Source (Villingen, Switzerland). Diffraction data were indexed and integrated using iMOSFLM (Battye, Kontogiannis, Johnson, Powell, & Leslie, 2011) and scaled using Aimless (Evans, 2011; Evans & Murshudov, 2013).The solutions for the bZiPro-compound 1/2/3 complex crystal structures were determined by molecular replacement with the program MOLREP and PHASER MR using bZiPro structure as a model (PDB code 5GPI) (McCoy, 2007; Vagin & Teplyakov, 2010). The twin laws for the data sets were determined using PHENIX Xtriage (Adams et al., 2010). The structure was subjected to iterative rounds of refinement using the PHENIX refine with twin law (k, h, -l) applied and manual rebuilding using Coot (Afonine et al., 2012; Emsley & Cowtan, 2004). The final data collection and refinement statistics are summarized in Table 1. Figures were generated using PyMOL (DeLano, 2004, 2009).

2.3 Inhibitor synthesis

Compounds 1-3 were originally designed as inhibitors of the WNV protease and prepared by solid phase peptide synthesis (SPPS) or by SPPS in combination with solution synthesis, as previously described (Kouretova et al., 2017).

2.4 Inhibition assays

The inhibition assays were carried as previously described (Phoo et al., 2016; Zhang et al., 2016). In short 3 nM final concentration of bZiPro was incubated with varying concentrations of inhibitors for 5 minutes and 30 minutes at room temperature in assay buffer (20 mM Tris pH 8.5, 10% glycerol, 0.01% Triton X-100, 2mM DTT). Upon addition of the fluorogenic substrate benzoyl-nKRR-AMC (assay concentration 10 µM), the initial velocities were measured at 37 °C at λ_{ex} at 380 nm and λ_{em} at 460 nm every sixty seconds over a period of 12 minutes using Cytation 3 Multimode plate reader (BioTek Instruments). Inhibition assays were performed as triplicates. The determined initial velocities were normalized (control in absence of inhibitor set to 100 %) and plotted as a function of the inhibitor concentrations (Figure 1). The data were analysed by nonlinear regression using GraphPad Prism. The IC_{50} values were calculated by using the Log (inhibitor): normalized response function implemented, in GraphPad Prism version 5.0 (GraphPad Software, La Jolla California, USA).

2.5 Mass spectrometry analysis

The inhibitors were incubated with bZiPro at 10:1 ratio (inhibitor: bZiPro) for 4 hours at 37 °C. The same concentration of each inhibitor without bZiPro was prepared as negative controls. Analytical reverse phase chromatography was performed using ACQUITY UPLC BEH C18 column, 2.1 X 100 mm (Waters, USA), thermostated at 65 °C, with an Acquity H-Class UPLC coupled to UPLC PDA and QDa Mass Detector (Waters, USA), with Mobile phase A in ultrapure water containing 0.1% formic acid and mobile phase B in methanol containing 0.1% formic acid. The mobile phase was delivered at a flow rate of 0.4 mL/min with the following gradient: 0 – 2 min, 10 % B; 2 – 4 min, 80 % B; 4 – 6 min, 80 % B; followed by a return to 10 % B at 9 min. Absorption was measured at 280

nm and 260 nm. The QDa ESI source was operated in positive mode, capillary voltage of 0.8 V, cone voltage of 10 V, probe temperature at 600 °C, over a scan range of 150 – 1250 m/z at a frequency of 8 Hz. The chromatograms and mass spectra were acquired and analyzed using Waters Masslynx 4.1 and deconvoluted using MaxEnt1.

3. Results

3.1 Inhibition of bZiPro by the peptidomimetic compounds

We determined the half maximal inhibitory concentration (IC_{50}) of the three peptidomimetic inhibitors with different P1′ and P4 groups (Figure 1A-C). The IC_{50} values of compounds 1, 2 and 3 are found to be in low micromolar range, 1.2 ± 0.14 µM, 1.6 ± 0.14 µM and 1.1 ± 0.07 µM respectively (Figure 1A-C). The K_i values of the inhibitors are calculated based on Cheng-Prusoff equation and they are 0.047 µM, 0.06 µM and 0.43 µM for compound 1, 2 and 3 respectively (Cheng & Prusoff, 1973). Due to the substrate analogue structures containing various P1′ groups, we hypothesized that bZiPro might be able to cleave these inhibitors. To investigate this, the molecular weight of the compounds before and after incubation with bZiPro was determined using ESI-MS (Figure 2). The analysis revealed that compounds 1 and 2 were cleaved after the P1 Arg residue by bZiPro (Figure 2A-D). For the peptide 1 the molecular weight was decreased by 113 Daltons after incubation, indicating the removal of the C-terminal Gly-Gly-NH_2 segment (Figure 2A-B). Incubation of compound 2 with bZiPro resulted in a mass increase of 1 Dalton, implying that the C-terminal amide moiety was converted to a carboxyl group (Figure 2C-D). In contrast, compound 3 did not show any change in molecular weight, suggesting that the Arg-4-Amba bond is resistant to cleavage by bZiPro (Figure 2E-F). We have determined the IC_{50} values of the inhibitors with longer incubation time (30 minutes) (Figure S1) and found that the IC_{50} values vary less than 10% for the compound 2 and 3 (Figure S1B-C). For compound 1, the IC_{50} value increased two folds when the incubation time was extended to 30 minutes (Figure S1A). We also synthesized the peptides after cleavage of compound 1 and 2 by bZiPro (compound 1B and 2B) and determined their inhibitory potencies after 5 minutes of incubation with bZiPro (Figure 1D-E). As expected, the IC_{50} values are significantly higher than those of the compounds before cleavage. The difference is more striking for compound 1 and 1B as the IC_{50} value of compound 1B is 18.4 ± 1.9 µM which is 15 times higher than for compound 1 (Figure 1A and 1D). The IC_{50} value of compound 2B (5.9 ± 0.55 µM) is 3.5 times higher compared to inhibitor 2 (Figure 1B and 1E). The K_i values of the compound 1B and 2B are 7.13 µM and 2.29 µM respectively.

3.2 Crystal structures of ZIKV protease in complex with compound 1, 2 or 3

The co-crystal structures of bZiPro (C143S) with compounds 1, 2 or 3 were determined at a resolution of 2 Å, 1.8 Å and 1.7 Å, respectively (Figure 3A, S1, and S2). The data collection and refinement statistics are summarized in Table 1. For all three co-crystal structures, there are four bZiPro molecules in one asymmetric unit (ASU) with almost same conformation (RMSD < 0.4 Å for 160 Cα atoms). In all three co-crystal structures, only two out of four bZiPro molecules in one ASU are occupied by the inhibitor (Figure S4).

3.3 Detailed interactions between bZiPro and compound 1

The P1′-P2′ Gly-Gly-NH_2 segment of the inhibitor is not observed in the co-crystal structure (Figure 3B), indicating that bZiPro cleaved compound 1 after the P1 arginine. This observation is consistent with the result of mass spectrometry analysis (Figures 2A and 2B). One of the C-terminal carboxyl oxygen atoms of P1 Arg interacts with the amide nitrogens of S135 and G133 of the oxyanion hole, whereas the second oxygen forms a H-bond to the imidazole nitrogen of His51 in a similar fashion to the structure of bZiPro in complex with Acetyl-Lys-Arg-H (Li et al., 2017). Moreover, the P1 amide NH forms a close contact to the carbonyl oxygen of G151. Notably, the side chain of S135 is pointing away from the negatively charged P1 carboxylate group. One of the terminal guanidine nitrogens of P1 Arg interacts with the D129 side chain and carbonyl oxygen of Y130. The P2 Lys binds to the carbonyl oxygen of G82 and D83 side chain of NS2B. The P3 Lys side chain makes polar contacts to the carbonyl oxygen of F84 and the S85 hydroxyl group of NS2B, while the P3 backbone carbonyl oxygen is bound to the hydroxyl group of Y161 and the amide NH of G153. Moreover, the P4 backbone carbonyl forms two H-bonds to the guanidine group of the P1 Arg (Figure S5A-B). These contacts may stabilize the horseshoe-like overall backbone conformation of the bound inhibitor (Figure 3B, Figure S5A-B).

3.4 Detailed interactions between bZiPro and compound 2

In the co-crystal structure (Figure 3C), the C-terminus of compound 2 was built as carboxyl group, in agreement with the mass spectrometry results (Figure 2C-D). The two compounds at each active site

interact similarly with bZiPro for P1 and P3 residues. The P2 backbone nitrogen and P4 cap moiety adopt slightly different conformations in the two bound molecules of compound 2 (Figure S4A-B, Figure S5A-B). In Figure 3, the complex with better electron density map is displayed. The electron density maps for both compounds are shown in Figure S4A-B. Out of two compound 2 molecules, one of the P2 backbones is similarly oriented as the P2 backbone of compound 1, whereas the other is similarly placed as in the compound 3 complex (Figure S4A-B, Figure S5A-B). The first conformation interacts with G151, while the second conformation does not. In both conformations, the P2-Lys side chain makes contacts with the carbonyl oxygen of G82 and N152 side chain. The P3 backbone carbonyl oxygen interacts with Y161 and G153 similar to the bZiPro-compound 1 complex, while the P3-Lys side chain is bound to the carbonyl oxygen of F84 of NS2B. However, unlike the bZiPro-compound 1 complex; no polar contact to the side chain of S85 exists.. The amide bond between the P3 Lys and P4 4-GMe-Phac group is rotated and the P4 carbonyl oxygen cannot form any intramolecular interaction with the P1 guanidino group as observed in the bZiPro-compound 1 complex. Instead, the P4 guanidine group interacts with E62 of a neighboring NS2B molecule, which might cause the rotation of the P3-P4 amide backbone (Figure 3C, Figure S5B). In contrast, the second bZiPro-compound 2 molecule does not contact with the neighboring NS2B molecule and forms an intramolecular contact between the P4 and the P1 group (Figure S5C, D).

3.5 Detailed interactions of bZiPro with compound 3

In contrast to the two other complexes, the P1-P1′ peptide bond of compound 3 is stable and not cleaved by bZiPro as can be observed in the co-crystal structure (Figure 3D) . The electron density for the P1′ 4-amidinobenzylamide group is clearly visible; the stability of the inhibitor is also supported by the mass spectrometry results (Figure 2C, Figure S4). The P1 Arg residue binds in a similar fashion as described in the complexes with compounds 1 and 2. Here, the P2-Arg side chain interacts with G82 and S81 of NS2B. Since Arg at P2 residue forms additional interactions with the protease, it may be better suited than Lys for the design of substrate-analogue inhibitors of bZiPro. In contrast, the P2 backbone does not form any polar interactions to the protease. The backbone carbonyl oxygen of P3 Arg forms similar hydrogen bonds with Y161 and G153 as found in the other two complexes.

The P4 4-GMe-Phac moiety points out of the substrate binding pocket, whereas its guanidine group makes a salt bridge (2.8 Å) to the carboxyl group of D129. Moreover, its phenyl ring partially covers the P1 side chain and is probably involved in intramolecular cation-π interactions to the P1 guanidino group. This horseshoe-like conformation of the inhibitor backbone is further stabilized by a hydrogen bond between the P4 carbonyl oxygen and the guanidine of the P1 Arg residue (Figure S5E-F). The P1′ 4-amidinobenzylamide group is occupying the shallow subpocket next to the S1 site lined by V36, V52 and A132-G133, whereas the polar amidine substituent is directed towards the solvent (Figure 3D, Figure S5E and F).

3.6 Comparison of the bZiPro-compound 3 complex with structures of other flavivirus proteases bound to various peptidic inhibitors

The comparison of the bZiPro-compound 3 complex with previously reported structures of DENV, WNV and ZIKV proteases with peptidic inhibitors shows that the overall fold is similar in all structures (Figure 4 and Supplementary Table 1). Multiple sequence alignment showed mostly conserved S1 pocket residues; therefore, it is not surprising that the P1 Arg from different peptidic inhibitors interacts with the same NS3 residues. In contrast, the S2 and S3 pockets are formed by residues from both NS2B and NS3. Slightly different residues in the NS2B cofactor sequence (residues 80-83) could be the reason for slight variations in the preferred P2 and P3 residues among the different flavivirus proteases. The superimposition of bZiPro-compound 3 with the bZiPro-TGKR peptide structure shows similar P1 interactions with similar P1-P3 backbone conformation (Figure 4C). Superimposition of the structure of compound 1, 2 and 3 when bound to bZiPro showed that the P4 groups of different inhibitors occupy the S4 pocket in slightly different orientations. This indicates that the S4 pocket is not fully occupied and it might be possible to include even larger and/or more bulky P4 residues. We speculate that this could improve the potency and cellular permeability of this inhibitor type.

4. Discussion

Several structures of the ZIKV protease in complex with dipeptides or small molecule fragments have been reported (Lei et al., 2016; Li et al., 2018; Li et al., 2017; Phoo et al., 2016).The two dipeptide compounds reported by Lei et al. and Li et al. form covalent but reversible adducts with the catalytic serine (Lei et al., 2016; Li et al., 2017). In the known bZiPro and eZiPro structures from former studies, the S3 pocket is largely unoccupied (Phoo et al., 2016; Zhang et al., 2016). To explore the substrate/inhibitor binding to the all of S1-S4 pockets, we determined the crystal structures of unlinked ZIKV NS2B-NS3 protease in complex with three reversible peptidomimetic inhibitors. Overall, binding of substrates or inhibitors do not induce significant conformational changes in the protease indicated by low RMSD values (Supplementary Table 1, Figure S2, and Figure S3). The P3-P1 backbones of the three compounds are orientated relatively similarly amongst themselves (Figure 4A) and to the tetrapeptide TGKR in the eZiPro structure (Figure 4C). At P2 position, an arginine side chain can make more contacts with bZiPro as compared with lysine. For P3, both lysine and arginine form similar interactions with bZiPro. The different conformations of the used P4 moieties in the co-crystal structures indicate that the P4 group has a higher degree of conformational freedom. This could allow the incorporation of different P4 moieties to improve the potency or drug-like properties. Of the three compounds, inhibitor 3 has the strongest potency against bZiPro. Its P4 4-guanidinomethyl-phenylacetyl-group is shielding the P1 side chain similarly to the 3,4-dichlorophenylacetyl- group in complex with the WNV protease (Figure 4D) (PDB ID: 2YOL) (Hammamy et al., 2013). It is noteworthy that in this WNV inhibitor a trans-(4-guanidino)cyclohexylamide (GCMA) residue was incorporated as P1 residue, which represents a decarboxylated Arg mimetic. Interestingly, the cyclic boronate diester of cn-716 reported by Lei et al. also occupies the same shallow S1′ region as found for the 4-Amba residue in the complex with compound 3 (Figure 4B) (Lei et al., 2016). The P1-P1′ bond of compound 3 is not hydrolysable by bZiPro which might explain the slightly better potency of this inhibitor. An additional cause for the improved IC_{50} value of compound 3 could be attributed to the P2 Arg side chain, which enables more

contacts to bZiPro than P2 Lys, as well as to the N-terminal group in P4 position forming an additional salt bridge to the D129 side chain.

Due to their tribasic P3-P1-segment the used compounds 1-3 possess a limited selectivity and show micromolar activity against the WNV and DENV proteases in *in vitro* assays (Kouretova et al., 2017). Moreover, the incorporation of the C-terminal 4-Amba cap in compound 3 also leads to a very potent inhibitor of the proprotein convertase furin with an inhibition constant of 57 pM (Kouretova et al., 2017). Notably, all of these compounds showed negligible efficacy in cell-based assays against WNV and DENV, possibly due to poor cellular permeability or insufficient potency (Kouretova et al., 2017). Moreover, incubation of compounds 1 and 2 with the WNV protease at identical concentrations as used in the kinetic measurements, followed by subsequent HPLC analysis revealed only a minor cleavage of these derivatives during a period of 4 hours (Kouretova et al., 2017). Therefore, it was assumed that the inhibitory potency against the WNV enzyme during the kinetic measurement of 20 minutes was mainly caused by the intact compounds and not by the cleaved P4-P1 product. However, the lack of co-crystal structures for the WNV protease in complex with these compounds makes it challenging to predict differences in the binding mode of both compounds in the active site of the WNV and ZIKV protease to explain the different cleavage efficiencies.

In structure-based drug discovery, characterizing the active site of target proteins with various compounds is vital for the further optimization of lead structures. In this study, x-ray crystallography together with biochemical assays and mass spectrometry analysis was used to characterize the S4-S1′ binding pockets of the unlinked ZIKV NS2B-NS3 protease, bZiPro. We have also demonstrated that presence of a P1′ group could improve the potency of these petidic inhibitors. Furthermore, we conclude that the incorporation of larger hydrophobic P4 groups, for instance a biphenylacetyl residue, could improve the cellular permeability of this inhibitor class.

Acknowledgements

We thank Drs. Liew Chong Wai and El Sahili Abbas for the help with diffraction data collection. We acknowledge SOLEIL for provision of synchrotron radiation facilities (proposals ID 20170003) in using Proxima beamlines. We thank scientists and staff from Australian Light Source MX beam-line, Taiwan Photon Source beamline 05A, Swiss Light Source PX beam-line, and Proxima 2A Beamline, SOLEIL for their expert assistance with diffraction data collection. We thank Ms Hai Ning Pee and colleagues from Waters Pacific Pte Ltd for their technical support in the UPLC installation and use. This work was supported by (1) a start-up grant from Lee Kong Chian School of Medicine, Nanyang Technological University, (2) National Medical Research Council grant CBRG15May045, (3) National Research Foundation grant NRF2016NRF-CRP001-063, (4) MOE2016-T2-2-097 grant to D.L. and a grant by the German Center for Infection Research [DZIF–TTU 01.902] to T.S. T. S. obtained funding from the LOEWE Center DRUID (Novel Drug Targets against Poverty-Related and Neglected Tropical Infectious Diseases).

References

Adams, P. D., Afonine, P. V., Bunkoczi, G., Chen, V. B., Davis, I. W., Echols, N., . . . Zwart, P. H. (2010). PHENIX: a comprehensive Python-based system for macromolecular structure solution. *Acta Crystallogr D Biol Crystallogr, 66*(Pt 2), 213-221. doi:10.1107/S0907444909052925

Afonine, P. V., Grosse-Kunstleve, R. W., Echols, N., Headd, J. J., Moriarty, N. W., Mustyakimov, M., . . . Adams, P. D. (2012). Towards automated crystallographic structure refinement with phenix.refine. *Acta Crystallogr D Biol Crystallogr, 68*(Pt 4), 352-367. doi:10.1107/S0907444912001308

Aleshin, A. E., Shiryaev, S. A., Strongin, A. Y., & Liddington, R. C. (2007). Structural evidence for regulation and specificity of flaviviral proteases and evolution of the Flaviviridae fold. *Protein Sci, 16*(5), 795-806. doi:10.1110/ps.072753207

Baronti, C., Piorkowski, G., Charrel, R. N., Boubis, L., Leparc-Goffart, I., & de Lamballerie, X. (2014). Complete coding sequence of zika virus from a French polynesia outbreak in 2013. *Genome Announc, 2*(3). doi:10.1128/genomeA.00500-14

Battye, T. G., Kontogiannis, L., Johnson, O., Powell, H. R., & Leslie, A. G. (2011). iMOSFLM: a new graphical interface for diffraction-image processing with MOSFLM. *Acta Crystallogr D Biol Crystallogr, 67*(Pt 4), 271-281. doi:10.1107/S0907444910048675

Bell, B. P., Boyle, C. A., & Petersen, L. R. (2016). Preventing Zika Virus Infections in Pregnant Women: An Urgent Public Health Priority. *Am J Public Health, 106*(4), 589-590. doi:10.2105/AJPH.2016.303124

Cahour, A., Falgout, B., & Lai, C. J. (1992). Cleavage of the dengue virus polyprotein at the NS3/NS4A and NS4B/NS5 junctions is mediated by viral protease NS2B-NS3, whereas NS4A/NS4B may be processed by a cellular protease. *J Virol, 66*(3), 1535-1542.

Chambers, T. J., Grakoui, A., & Rice, C. M. (1991). Processing of the yellow fever virus nonstructural polyprotein: a catalytically active NS3 proteinase domain and NS2B are required for cleavages at dibasic sites. *J Virol, 65*(11), 6042-6050.

Chambers, T. J., Nestorowicz, A., Amberg, S. M., & Rice, C. M. (1993). Mutagenesis of the yellow fever virus NS2B protein: effects on proteolytic processing, NS2B-NS3 complex formation, and viral replication. *J Virol, 67*(11), 6797-6807.

Chambers, T. J., Weir, R. C., Grakoui, A., Mccourt, D. W., Bazan, J. F., Fletterick, R. J., & Rice, C. M. (1990). Evidence That the N-Terminal Domain of Nonstructural Protein Ns3 from Yellow-Fever Virus Is a Serine Protease Responsible for Site-Specific Cleavages in the Viral Polyprotein. *Proc Natl Acad Sci U S A, 87*(22), 8898-8902. doi:DOI 10.1073/pnas.87.22.8898

Chandramouli, S., Joseph, J. S., Daudenarde, S., Gatchalian, J., Cornillez-Ty, C., & Kuhn, P. (2010). Serotype-specific structural differences in the protease-cofactor complexes of the dengue virus family. *J Virol, 84*(6), 3059-3067. doi:10.1128/JVI.02044-09

Cheng, Y., & Prusoff, W. H. (1973). Relationship between the inhibition constant (K1) and the concentration of inhibitor which causes 50 per cent inhibition (I50) of an enzymatic reaction. *Biochem Pharmacol, 22*(23), 3099-3108.

Clum, S., Ebner, K. E., & Padmanabhan, R. (1997). Cotranslational membrane insertion of the serine proteinase precursor NS2B-NS3(Pro) of dengue virus type 2 is required for efficient in vitro processing and is mediated through the hydrophobic regions of NS2B. *J Biol Chem, 272*(49), 30715-30723.

de la Cruz, L., Nguyen, T. H., Ozawa, K., Shin, J., Graham, B., Huber, T., & Otting, G. (2011). Binding of low molecular weight inhibitors promotes large conformational changes in the dengue virus NS2B-NS3 protease: fold analysis by pseudocontact shifts. *J Am Chem Soc, 133*(47), 19205-19215. doi:10.1021/ja208435s

DeLano, W. L. (2004). Use of PYMOL as a communications tool for molecular science. *Abstracts of Papers of the American Chemical Society, 228*, U313-U314.

DeLano, W. L. (2009). PyMOL molecular viewer: Updates and refinements. *Abstracts of Papers of the American Chemical Society, 238*.

Emsley, P., & Cowtan, K. (2004). Coot: model-building tools for molecular graphics. *Acta Crystallographica Section D-Biological Crystallography, 60*, 2126-2132. doi:10.1107/S0907444904019158

Erbel, P., Schiering, N., D'Arcy, A., Renatus, M., Kroemer, M., Lim, S. P., . . . Hommel, U. (2006). Structural basis for the activation of flaviviral NS3 proteases from dengue and West Nile virus. *Nat Struct Mol Biol, 13*(4), 372-373. doi:10.1038/nsmb1073

Evans, P. R. (2011). An introduction to data reduction: space-group determination, scaling and intensity statistics. *Acta Crystallogr D Biol Crystallogr, 67*(Pt 4), 282-292. doi:10.1107/S090744491003982X

Evans, P. R., & Murshudov, G. N. (2013). How good are my data and what is the resolution? *Acta Crystallogr D Biol Crystallogr, 69*(Pt 7), 1204-1214. doi:10.1107/S0907444913000061

Hammamy, M. Z., Haase, C., Hammami, M., Hilgenfeld, R., & Steinmetzer, T. (2013). Development and characterization of new peptidomimetic inhibitors of the West Nile virus NS2B-NS3 protease. *ChemMedChem, 8*(2), 231-241. doi:10.1002/cmdc.201200497

Kang, C., Keller, T. H., & Luo, D. (2017). Zika Virus Protease: An Antiviral Drug Target. *Trends Microbiol, 25*(10), 797-808. doi:10.1016/j.tim.2017.07.001

Kim, Y. M., Gayen, S., Kang, C., Joy, J., Huang, Q., Chen, A. S., . . . Keller, T. H. (2013). NMR analysis of a novel enzymatically active unlinked dengue NS2B-NS3 protease complex. *J Biol Chem, 288*(18), 12891-12900. doi:10.1074/jbc.M112.442723

Koh-Stenta, X., Joy, J., Wang, S. F., Kwek, P. Z., Wee, J. L., Wan, K. F., . . . Nacro, K. (2015). Identification of covalent active site inhibitors of dengue virus protease. *Drug Des Devel Ther, 9*, 6389-6399. doi:10.2147/DDDT.S94207

Kouretova, J., Hammamy, M. Z., Epp, A., Hardes, K., Kallis, S., Zhang, L., . . . Steinmetzer, T. (2017). Effects of NS2B-NS3 protease and furin inhibition on West Nile and Dengue virus replication. *J Enzyme Inhib Med Chem, 32*(1), 712-721. doi:10.1080/14756366.2017.1306521

Lei, J., Hansen, G., Nitsche, C., Klein, C. D., Zhang, L., & Hilgenfeld, R. (2016). Crystal structure of Zika virus NS2B-NS3 protease in complex with a boronate inhibitor. *Science*. doi:10.1126/science.aag2419

Li, Y., Li, Q., Wong, Y. L., Liew, L. S., & Kang, C. (2015). Membrane topology of NS2B of dengue virus revealed by NMR spectroscopy. *Biochim Biophys Acta, 1848*(10 Pt A), 2244-2252. doi:10.1016/j.bbamem.2015.06.010

Li, Y., Zhang, Z., Phoo, W. W., Loh, Y. R., Li, R., Yang, H. Y., . . . Kang, C. (2018). Structural Insights into the Inhibition of Zika Virus NS2B-NS3 Protease by a Small-Molecule Inhibitor. *Structure*. doi:10.1016/j.str.2018.02.005

Li, Y., Zhang, Z., Phoo, W. W., Loh, Y. R., Wang, W., Liu, S., . . . Kang, C. (2017). Structural Dynamics of Zika Virus NS2B-NS3 Protease Binding to Dipeptide Inhibitors. *Structure, 25*(8), 1242-1250 e1243. doi:10.1016/j.str.2017.06.006

McCoy, A. J. (2007). Solving structures of protein complexes by molecular replacement with Phaser. *Acta Crystallogr D Biol Crystallogr, 63*(Pt 1), 32-41. doi:10.1107/S0907444906045975

Mueller, N. H., Yon, C., Ganesh, V. K., & Padmanabhan, R. (2007). Characterization of the West Nile virus protease substrate specificity and inhibitors. *Int J Biochem Cell Biol, 39*(3), 606-614. doi:10.1016/j.biocel.2006.10.025

Nitsche, C., Zhang, L., Weigel, L. F., Schilz, J., Graf, D., Bartenschlager, R., . . . Klein, C. D. (2017). Peptide-Boronic Acid Inhibitors of Flaviviral Proteases: Medicinal Chemistry and Structural Biology. *J Med Chem, 60*(1), 511-516. doi:10.1021/acs.jmedchem.6b01021

Noble, C. G., Seh, C. C., Chao, A. T., & Shi, P. Y. (2012). Ligand-bound structures of the dengue virus protease reveal the active conformation. *J Virol, 86*(1), 438-446. doi:10.1128/JVI.06225-11

Noble, C. G., & Shi, P. Y. (2012). Structural biology of dengue virus enzymes: towards rational design of therapeutics. *Antiviral Res, 96*(2), 115-126. doi:10.1016/j.antiviral.2012.09.007

Phoo, W. W., Li, Y., Zhang, Z., Lee, M. Y., Loh, Y. R., Tan, Y. B., . . . Luo, D. (2016). Structure of the NS2B-NS3 protease from Zika virus after self-cleavage. *Nat Commun, 7*, 13410. doi:10.1038/ncomms13410

Robin, G., Chappell, K., Stoermer, M. J., Hu, S. H., Young, P. R., Fairlie, D. P., & Martin, J. L. (2009). Structure of West Nile virus NS3 protease: ligand stabilization of the catalytic conformation. *J Mol Biol, 385*(5), 1568-1577. doi:10.1016/j.jmb.2008.11.026

Schuller, A., Yin, Z., Brian Chia, C. S., Doan, D. N., Kim, H. K., Shang, L., . . . Vasudevan, S. G. (2011). Tripeptide inhibitors of dengue and West Nile virus NS2B-NS3 protease. *Antiviral Res, 92*(1), 96-101. doi:10.1016/j.antiviral.2011.07.002

Shannon, A. E., Pedroso, M. M., Chappell, K. J., Watterson, D., Liebscher, S., Kok, W. M., . . . Young, P. R. (2016). Product release is rate-limiting for catalytic processing by the Dengue virus protease. *Sci Rep, 6*, 37539. doi:10.1038/srep37539

Vagin, A., & Teplyakov, A. (2010). Molecular replacement with MOLREP. *Acta Crystallogr D Biol Crystallogr, 66*(Pt 1), 22-25. doi:10.1107/S0907444909042589

Weigel, L. F., Nitsche, C., Graf, D., Bartenschlager, R., & Klein, C. D. (2015). Phenylalanine and Phenylglycine Analogues as Arginine Mimetics in Dengue Protease Inhibitors. *Journal of Medicinal Chemistry, 58*(19), 7719-7733. doi:10.1021/acs.jmedchem.5b00612

Yin, Z., Patel, S. J., Wang, W. L., Chan, W. L., Ranga Rao, K. R., Wang, G., . . . Keller, T. H. (2006). Peptide inhibitors of dengue virus NS3 protease. Part 2: SAR study of tetrapeptide aldehyde inhibitors. *Bioorg Med Chem Lett, 16*(1), 40-43. doi:10.1016/j.bmcl.2005.09.049

Yin, Z., Patel, S. J., Wang, W. L., Wang, G., Chan, W. L., Rao, K. R., . . . Keller, T. H. (2006). Peptide inhibitors of Dengue virus NS3 protease. Part 1: Warhead. *Bioorg Med Chem Lett, 16*(1), 36-39. doi:10.1016/j.bmcl.2005.09.062

Zhang, Z., Li, Y., Loh, Y. R., Phoo, W. W., Hung, A. W., Kang, C., & Luo, D. (2016). Crystal structure of unlinked NS2B-NS3 protease from Zika virus. *Science, 354*(6319), 1597-1600. doi:10.1126/science.aai9309

Table 1: Data collection and refinement statistics

	Compound 1 PDB id: 5ZMQ	Compound 2 PDB id: 5ZMS	Compound 3 PDB id: 5ZOB
Data collection			
Wavelength (Å)	1	1	1
Resolution range (Å)	60.33 - 1.99 (2.04-1.99)	27.42 - 1.80 (1.84-1.80)	42.97-1.70 (1.73-1.70)
Space group	P 2_1 2_1 2_1	P 2_1 2_1 2_1	P 2_1 2_1 2_1
Unit cell			
a, b, c (Å)	60.15, 60.33, 214.07	60.33, 60.35, 214.68	60.42, 60.42, 214.87
α,β,γ (°)	90, 90, 90	90, 90, 90	90, 90, 90
Total no of reflections	302087 (19285)	346043 (17660)	476930(22778)
Unique reflections	53862 (3829)	37988(2214)	87405(4443)
Multiplicity	5.6 (5.0)	9.1 (8.0)	5.5(5.1)
Completeness (%)	98.40% (92.10%)	99.9% (99.6%)	99.94% (100.00%)
I/σI	10.3 (2.9)	12 (1.5)	9.3(1.7)
Wilson B factor (Å²)	19.6	19.5	24.6
$CC_{1/2}$	0.99 (0.77)	0.99 (0.412)	0.99 (0.90)
R_{merge}[a]	0.09 (0.44)	0.109 (1.29)	0.065(0.68)
Refinement			
Resolution range (Å)	57.91 - 1.99 (2.06 - 1.99)	24.5 - 1.67 (1.70 - 1.67)	46.18 - 1.70 (1.76 - 1.70)
R_{factor}[b]	0.1705	0.2079	0.2572
R_{free}[c]	0.2012	0.2575	0.2791
No of non-hydrogen atoms			
Macromolecules	5615	5708	5801
Ligands	78	88	116

Water	499	420	243
RMSD (bonds) (Å)	0.003	0.67	0.002
RMSD (angles) (°)	0.685	0.003	0.68
Ramachandran favored (%)	97.0	93.4	94
Ramachandran allowed (%)	2.9	6.2	5.6
Ramachandran outliers (%)	0.1	0.4	0.4
Clash score	5.69	8.03	9.86
Average B factor (Å²)			
Macromolecules	21.72	31.01	27.80
Ligands	25.64	27.28	25.1
Solvent	35.3	34.54	28.40

*Statistics for the highest-resolution shell are shown in parentheses.

[a] $R_{merge} = \Sigma_h \Sigma_i |I_{hi} - \langle I_h \rangle| / \Sigma_{h,i} I_{hi}$, where I_{hi} is the i^{th} observation of the reflection h, while $\langle I_h \rangle$ is its mean intensity.

[b] $R_{factor} = \Sigma \, ||F_{obs}| - |F_{calc}|| \, / \, \Sigma \, |F_{obs}|$.

[c] R_{free} was calculated with 5% of reflections excluded from the whole refinement procedure.

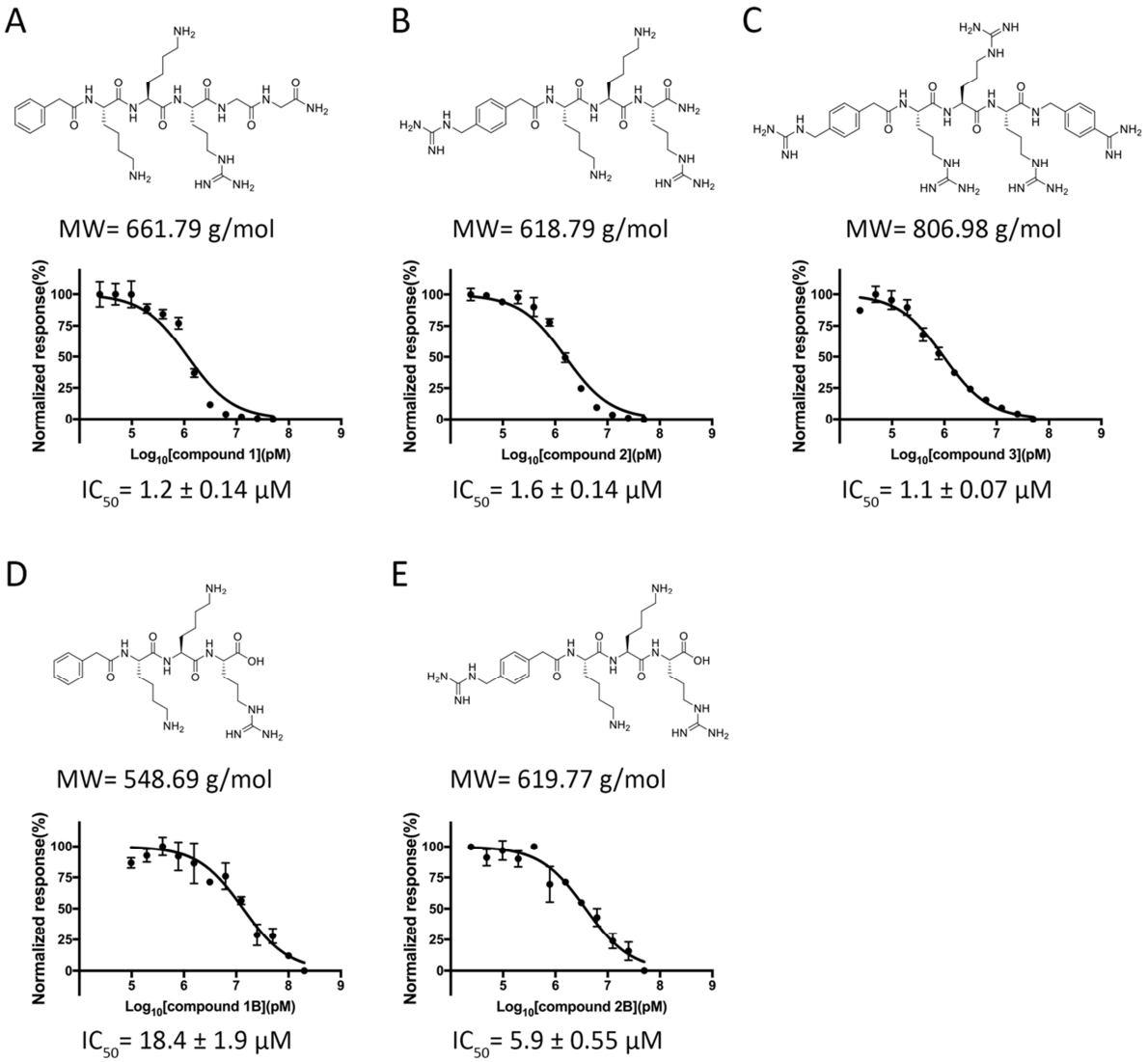

Figure 1. Structures of the inhibitors used in this study along with their half maximal inhibitory curves against the NS2B-NS3 protease of ZIKV using 10 µM benzoyl-nKRR-AMC as substrate (pH 8.5). The NS2B-NS3 protease and the inhibitors were incubated for 5 minutes at room temperature. The average molecular weights of the compounds are given below each structure. (A) Compound 1: Phenylacetyl-Lys-Lys-Arg-Gly-Gly-NH_2 (B) Compound 2: 4-guanidinomethyl-phenylacetyl-Lys-Lys-Arg-NH_2 (C) Compound 3: 4-guanidinomethyl-phenylacetyl-Arg-Arg-Arg-4-amidinobenzylamide. (D) Compound 1B: hydrolysis product of compound 1 (E) Compound 2B: hydrolysis product of compound 2. The error bars represent standard errors.

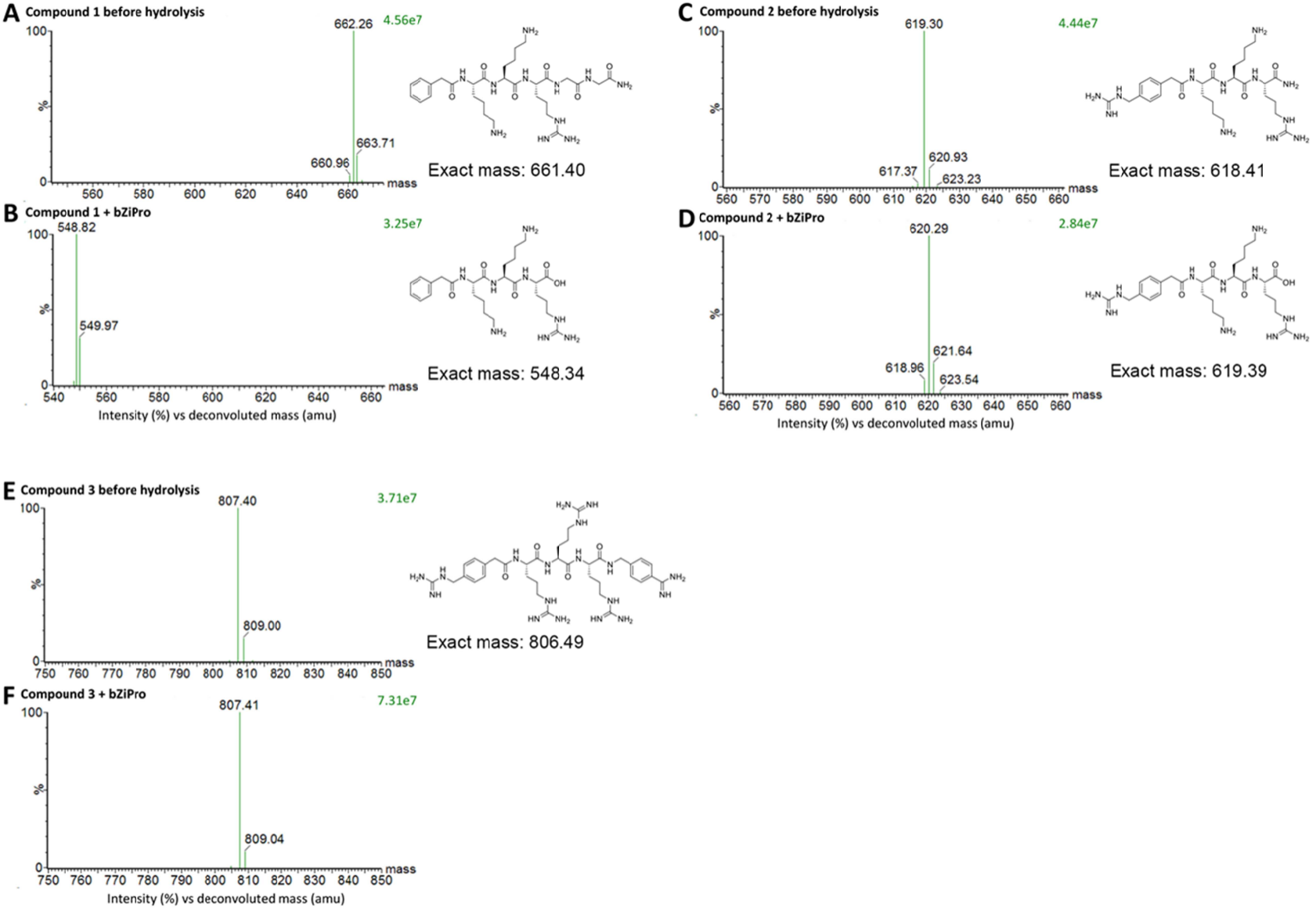

Figure 2. Mass spectra of the compounds before and after incubation with bZiPro determined by ESI-MS. The chemical structures of the compounds before and after hydrolysis are drawn next to the peak in addition to their exact weights. (A – B) Compound 1 is reduced by 110 Da after incubation with bZiPro. (C – D) For compound 2, the molecular weight is increased by 1 Da after cleavage of the C-terminal amide bond. (E – F) The molecular weight of compound 3 remained unchanged before and after incubation with bZiPro.

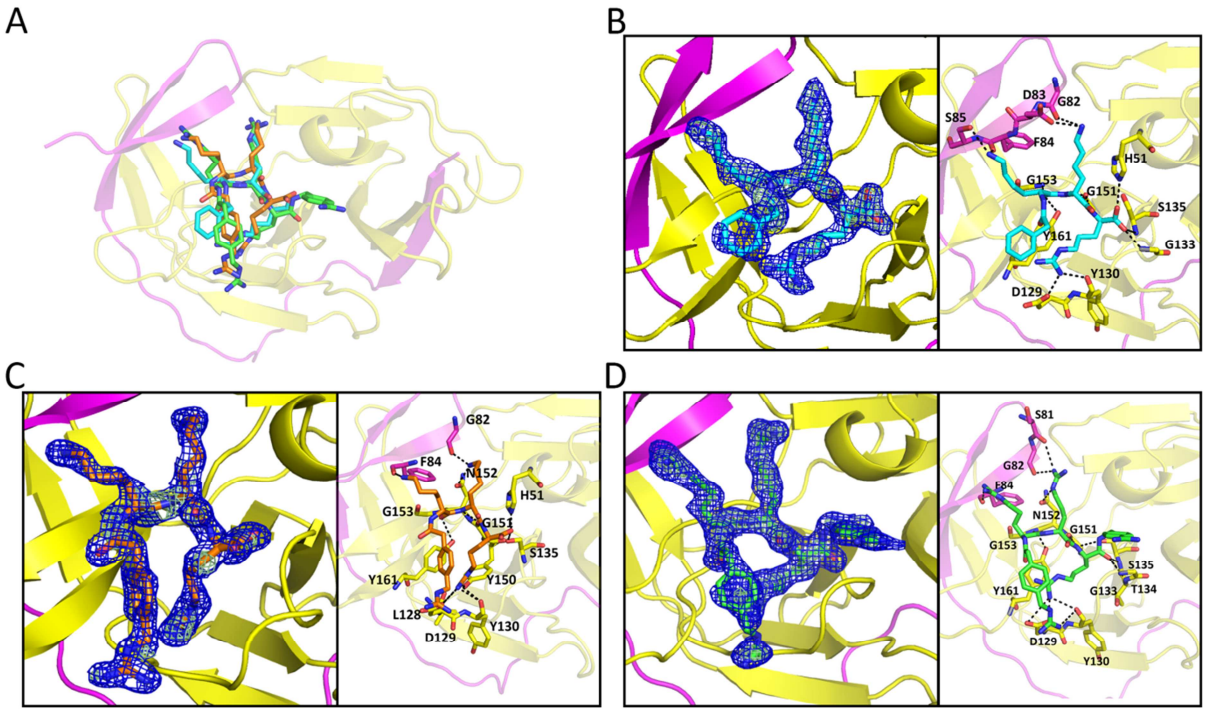

Figure 3. Crystal structures of bZiPro in complex with compounds 1, 2 and 3. (A) Overall conformation of bZiPro with compound 1, 2 and 3 in the active site. NS2B (magenta) and NS3 (yellow) are shown as ribbons while the P4-P1 segments of the cleaved compounds 1 (with cyan carbons) and 2 (orange), as well as the intact inhibitor 3 (green) are given in sticks representation. (B-D) The electron density maps and detailed interactions of compound 1 with bZiPro are shown in panel (B), of compound 2 in panel (C) and of compound 3 in panel (D). The electron density maps ($2mF_o$-F_c) in the left panels are colored in blue and contoured at 1σ and the omit map (mF_o-F_c) in green contoured at 3σ are shown The right panels in show the detailed interactions between the compounds and bZiPro. The involved bZiPro residues interacting with the compounds are shown as sticks and are labeled.

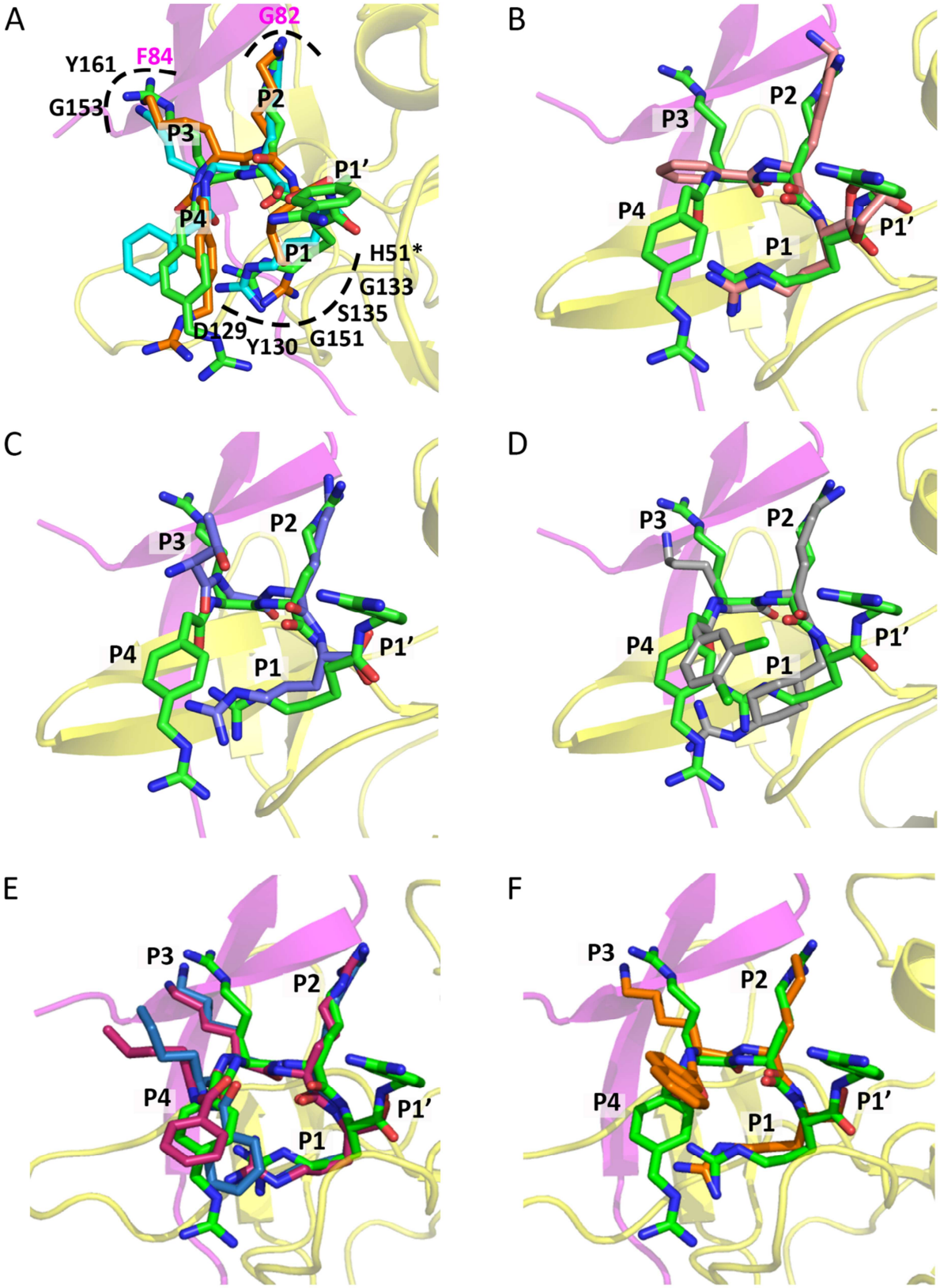

Figure 4. Superimposed structures of peptidic inhibitors in bZiPro, shown with its backbone in cartoon style with the (NS2B colored in magenta and NS3 in yellow). (A) Superimposition of cleaved compounds 1 (carbons in cyan) and, 2 (carbons in orange), with the intact inhibitor 3 (in all panels

with green C-atoms) in the active site of bZiPro. Conserved residues contributing to the binding of all three inhibitors are labeled. The P3-P1 residues from the three compounds make similar interactions with bZiPro, although the P2 Arg is slightly better suited than Lys at this position. The used P4 groups adopt slightly different positions indicating that the S4 pocket can be used for further optimization of the inhibitor. The P1′ 4-amidinobenzylamide group of compound 3 is not occupying the S1′ pocket and points toward the solvent. (B) Superimposition of the bZiPro in complex with -compound 3 with the bound structure of the boronic acid inhibitor cn-716 (carbons in light pink, PDB id: 5LC0). (C) Comparison of the structure of the bound compound 3 with the peptide TGKR (carbons in blue) after ZIKV NS2B-NS3 protease self-cleavage (PDB id: 5GJ4). (D) Comparison of the bound structure of compound 3 with the conformation of the bound inhibitor 3,4-dichloro-phenylacetyl-Lys-Lys-GCMA in the active site of the WNV protease (carbons in gray), (PDB id: 2YOL). (E) Comparison of the bound compound 3 with the structure of benzyol-Nle-Lys-Arg-Arg-H in complex with the- WNV protease (inhibitor with carbons in magenta) and with the DENV-3 protease (inhibitor with carbons in blue) structure (PDB id: 3U1I for DENV-3, 2FP7 for WNV). (F) Comparison of bound compound 3 in bZiPro with 2-naphthoyl-Lys-Lys-Arg-H in complex with the WNV NS2B-NS3 protease (carbons in orange) (PDB id: 3E90).

Highlights

- Crystal structures of unlinked ZIKV protease (bZiPro) with three peptide inhibitors at resolution of 2Å, 1.8Å and 1.9Å.
- The inhibitor 3 is the longest peptidic inhibitor co-crystallised with flaviviral protease.
- The susceptibility of the inhibitor for cleavage between P1 and P1' affects the inhibition efficiency of the compound.
- The structural characterisation of S4-S1 and -S1’ pockets reported here is useful for antivirals against ZIKV.